Island Arc

Island Arc (2014) **23,** 368–382

Research Article

Basaltic volcaniclastics from the Challenger Deep forearc segment, Mariana convergent margin: Implications for tectonics and magmatism of the southernmost Izu–Bonin–Mariana arc

Robert J. Stern,[1]* Minghua Ren,[2] Katherine A. Kelley,[3] Yasuhiko Ohara,[4,5] Fernando Martinez,[6] and Sherman H. Bloomer[7]

[1]*Geosciences Department, University of Texas at Dallas, 800 W. Campbell Road, Richardson, Texas 75080, USA (email: rjstern@utdallas.edu),* [2]*Department of Geosciences, University of Nevada Las Vegas, Las Vegas, Nevada 89154-4010, USA,* [3]*Graduate School of Oceanography, University of Rhode Island, Narragansett Bay Campus, Narragansett, Rhode Island, USA,* [4]*Hydrographic and Oceanographic Department of Japan, Tokyo 135-0064, Japan,* [5]*Japan Agency for Marine-Earth Science and Technology, Yokosuka 237-0061, Japan,* [6]*Hawai'i Institute of Geophysics and Planetology, SOEST, University of Hawai'i at Manoa, Honolulu, Hawaii, USA, and* [7]*Geosciences Department, Oregon State University, 128 Kidder Hall, Corvallis, Oregon 97331, USA*

Abstract Convergent margin igneous activity is generally limited to 100–200 km from the trench except where spreading ridges are subducted or in association with Subduction-Transform Edge Propagators (STEP faults). The southernmost Mariana forearc, facing the Challenger Deep, subducts Mesozoic seafloor and is not in a STEP fault setting but includes at least one site where tholeiitic basalts recently erupted close to the trench, the SE Mariana Forearc Rift (SEMFR). We present evidence of young basaltic volcanism from ca. 100 km west of SEMFR. Shinkai 6500 diving during YK13-08 (Dive 1363) recovered volcaniclastics from 5.5 to 6 km deep in the inner wall of the Mariana Trench, 50 km NE of the Challenger Deep. Glassy fragments are tholeiitic basalts similar to MORB except for much higher contents of magmatic water (approx. 2% H_2O vs. <0.2% H_2O in MORB) and enrichments in trace elements Rb-Cs-Ba, K, Pb, and Sr. Dive 1363 glasses are similar to basalts from SEMFR erupted near the trench and to Mariana Trough backarc basin basalts. Basalt fragments and palagonitized matrix dominate the studied samples, but small xenocrysts and xenoliths derived from mantle peridotite and Neogene volcanics are also present, probably torn from the vent walls. Dive 1363 hyaloclastites erupted at 3–6 km water depth accompanied by vigorous degassing of volatiles, most likely CO_2. These results provide further evidence that the forearc adjacent to the Challenger Deep has been invaded by asthenospheric mantle and derivative hydrous melts. Extension, hydration, and melt invasion combine to further weaken Challenger Deep forearc lithosphere. Combined effects of: (i) absence of strong, cold lithosphere of the overriding plate; (ii) rapid rollback of a narrow, short subducted slab; and (iii) weak coupling between the subducting Pacific plate and the overriding Mariana plate may be responsible for the great depth of the Challenger Deep.

Key words: basalt, Challenger Deep, Mariana Arc, subduction.

INTRODUCTION

The southernmost part of the approximately 1500 km-long Mariana arc system – where the Mariana Trench bends sharply west (Fig. 1A) – is a region that is tectonically active and poorly understood. Here, the Pacific Plate subducts almost orthogonally beneath the easternmost Philippine Sea (Mariana Plate) at about 30 mm/year (Fig. 1A; Bird 2003). Because the plate boundary trends E–W here, it interacts with the southernmost

*Correspondence.

Received 12 June 2014; accepted for publication 26 September 2014.

doi:10.1111/iar.12088

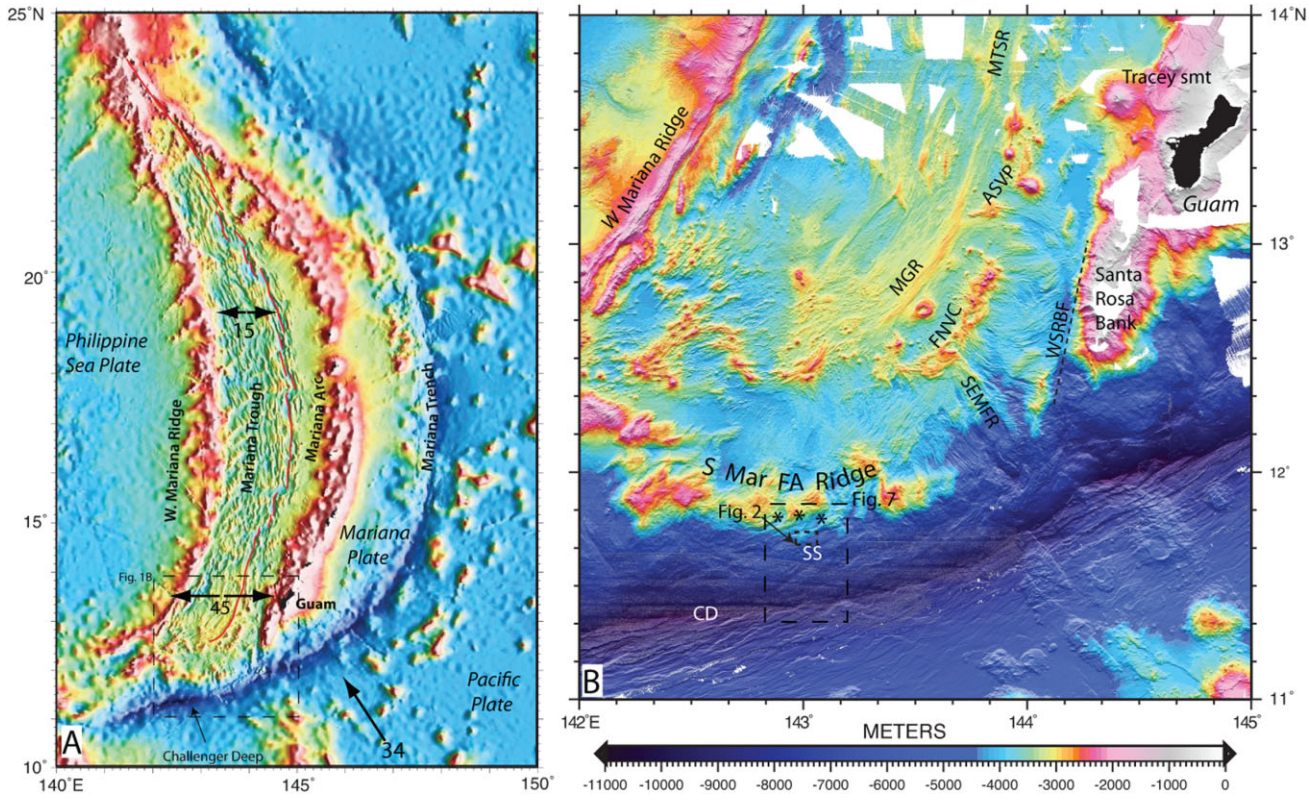

Fig. 1 Location of the study area. (A) Bathymetric map of the Mariana convergent margin in the Western Pacific, including Mariana Trench, Mariana Arc, and Mariana Trough (back-arc basin). Map was compiled from available bathymetric data including decimated one-minute grid for Mariana Trough (Kitada *et al.* 2006) Swath-mapped bathymetry is recompiled and matched to predicted bathymetry from Sandwell and Smith (1997). Red line is back-arc basin spreading axis from Martinez and Taylor (2003). Islands are black, the largest and southernmost is Guam, USA. Relative convergence of Pacific plate with Mariana plate is shown in mm/year, after Bird (2003). GPS-determined extension vectors for the Mariana Trough at the latitude of Guam and farther north are shown in mm/year, after Kato *et al.* (2003). Dashed box outlines region shown in (B). (B) Bathymetry of the southern Mariana Trough, showing location of spreading ridge (inflated Malaguana–Gadao Ridge (MGR) in the south, axial rift of Mariana Trough spreading ridge (MTSR) farther north) and Fina Nagu Volcanic Chain (FNVC), also West Santa Rosa Bank Fault (WSRBF), Alphabet Seamount Volcanic Province (ASVP), Southern Mariana Forearc Ridge (S Mar FA Ridge), Southeast Mariana Forearc Rift (SEMFR), Challenger Deep (CD), and Shinkai Seep (SS). The active magmatic arc southwest of Tracey Seamount is poorly constrained due to the unknown age of arc-like features (e.g. FNVC), but active volcanism is present from Tracey Seamount in the northeast to Toto caldera. Most data are from 'Law of the Sea' mapping carried out by the University of New Hampshire group (Armstrong 2011) with additional data from US-NGDC and JAMSTEC databases. Small dashed box shows study area in Figure 2, large dashed box shows HMR-1 sonar image area in Figure 7. Possible eruption sites are marked with '*'.

Mariana Trough, an actively spreading back-arc basin (BAB; Fig. 1A). This combination of strong convergence and extension is associated with the deepest point on Earth's solid surface, the Challenger Deep. It also causes the adjacent part of the Mariana Trough, just north of the Trench, to be seismically and magmatically active and to deform rapidly and complexly; GPS-determined extension rates increase southward in the Trough (Fig. 1A). We know from GPS studies that the southernmost Marianas (Fig. 1B) is the most rapidly deforming part of the 3000 km long Izu–Bonin–Mariana (IBM) arc system (Kato *et al.* 2003), but we are only beginning to understand how deformation and magmatism are distributed over this deeply submerged region.

Tectonics of the southernmost Marianas have a strong influence on the Mariana Trough BAB. Fryer (1995) first noted that the Mariana Trough had a different expression south of about 14°N and concluded that this reflected a different tectonic style in this region relative to that farther north. For most of its approximately 1200 km length, the Mariana Trough opens slowly E–W along a ridge system with slow-spreading axial valley morphology producing a variable but somewhat thin (3.5–4 km) volcanic crust estimated from gravity and bathymetry values (Kitada *et al.* 2006). South of about 14°N the spreading center bends increasingly westward and develops a fast-spreading axial-high morphology, although actual spreading rates are likely not high (Martinez *et al.* 2000). Gravity data suggest somewhat thicker crust in this area (6–7 km) (Kitada *et al.* 2006). The complexly deformed region – which we call the Southernmost Mariana Trough–Trench Complex

(SMTTC) – is delimited on the east by the West Santa Rosa Bank Fault (WSRBF) Fryer *et al.* (2003). The WSRBF can be traced as a >5 km scarp south of 13°N, diminishing in relief northwards until it is replaced by a northeast-trending fault scarp south of Tracey Seamount (Fig. 1B). The northern limit of the region affected by SMTTC tectonics lies at about 13°30′N, approximately where the Mariana volcanic front loses definition southward. This is also about where the BAB spreading center changes from an axial rift in the north into the inflated Malaguana–Gadao Ridge (MGR; Fig. 1B), which is underlain by the only known magma chamber in the Mariana Trough BAB (Becker *et al.* 2010). The Southern Mariana Forearc Ridge (Fig. 1B) separates the Mariana Trough to the north from the trench and Challenger Deep to the south; where this ridge has been sampled, it is composed of Miocene arc volcanics (M. Reagan, personal communication 2014).

More evidence that the SMTTC is unusually active comes from how the locus of arc volcanism is disrupted in this region. For approximately 2500 km north from Tracey seamount (about 13°40′N) all the way to Japan, discrete and well-developed volcanoes of the IBM active arc define a pronounced string of stratovolcanoes that is separated from the trench by a broad (approx. 150–200 km wide) forearc. As is characteristic for other magmatic arcs, IBM arc volcanoes are typically found about 100–150 km above the subducted Pacific Plate. Such a line of discrete, long-lived volcanoes is typical for mature convergent margins and is known as the 'magmatic front' (Matsuda & Uyeda 1971). The magmatic front marks where fluids and sediment melts released from the subducting plate trigger melting of convecting asthenosphere, and arc volcanoes build up over time where these melts rise to the surface. South of Tracey seamount, the line of arc volcanoes is poorly defined (Fig. 1B, Stern *et al.* 2013), despite the fact that the southern Mariana Trough is underlain by a subducted slab that can be traced to 150 km depth (Gvirtzman & Stern 2004). Poor definition of the magmatic arc SW of 13°40′N reflects tectonic instability in the SMTTC. Multiple sites of extension frequently divert the supply of arc magmas, not allowing magma supply to focus beneath discrete volcanoes so that these can grow to become large stratovolcanoes, as is seen for the arc to the north (Stern *et al.* 2013).

Complex deformation in the SMTTC reflects three interacting causes: (i) subduction of the Pacific Plate, which induces asthenospheric convection at the same time causing magma and fluids to be supplied to the overlying mantle, causing flux melting; (ii) BAB opening, which keeps lithosphere thin and causes decompression melting; and (iii) rapid rollback of a subducted slab that is narrow (from side to side) and short (from trench to downdip end of slab), which adds trench-normal extensional stresses to the overriding plate. The last point is especially important, because narrow slabs are thought to be able to roll back more rapidly than wide slabs (e.g. Dvorkin *et al.* 1993). Furthermore, Gvirtzman and Stern (2004) concluded that the plate-coupling zone along the Challenger Deep forearc segment was unusually narrow, only 50 km wide compared to approximately 150 km wide beneath the forearc farther north. The unusually narrow plate coupling zone allows convecting asthenosphere to penetrate closer to the trench than is found for other forearcs, and this allows the asthenosphere to be fluxed by shallow, slab-derived hydrous fluids and melt (Ribeiro *et al.* 2013a,b). The result is an unusually weak forearc that is volcanically active much closer to the trench than normally occurs.

It is not easy to identify where igneous activity occurs in this complexly deforming region. The Southeast Mariana Forearc Rift (SEMFR) marks one such region of forearc igneous activity, floored by 2.7–3.7 Ma low-K tholeiitic basalts (Ribeiro *et al.* 2013a,b). SEMFR lavas were produced by partial melting of a BAB-like mantle source, metasomatized by sediment melt and aqueous fluids released from dehydration of the subducted oceanic crust. SEMFR melts were probably generated when the Mariana Trough BAB first began to open in this region. But where else does igneous activity occur in this enigmatic and complexly-deforming region, and how close to the trench does igneous activity occur? In this contribution we present new evidence that MORB-like basalts with subtle arc signatures recently erupted very close to the trench, approximately 100 km west of SEMFR.

SAMPLE COLLECTION

Regional multibeam bathymetry in the area was obtained by the US Law of the Sea mapping project (Armstrong 2011) as well as on R/V Yokosuka (Fig. 2A). In Dec. 2011 to Jan. 2012 R/V Thomas G Thompson obtained two swaths of deep-towed (approx. 500 m altitude) IMI-30 sidescan

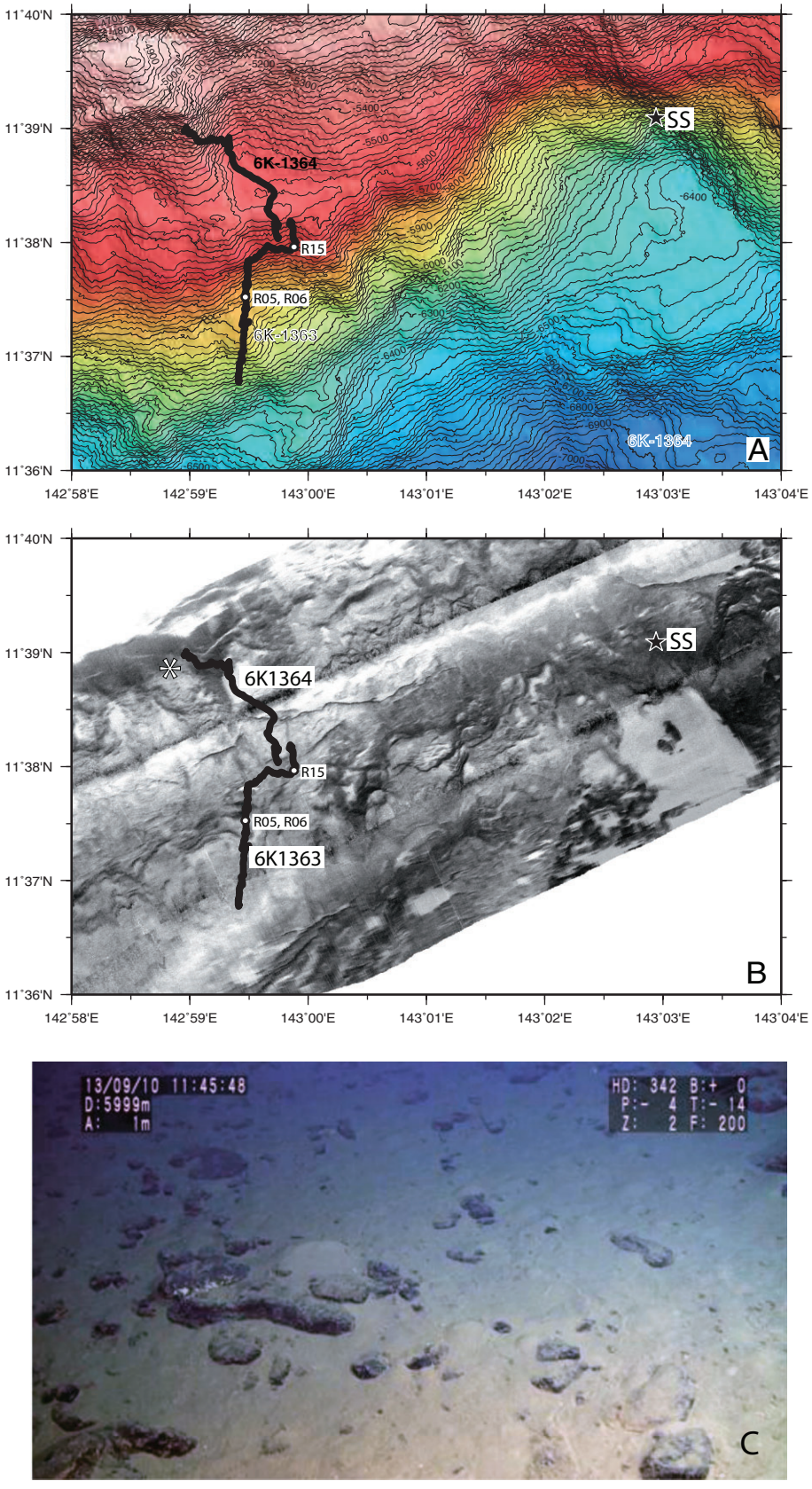

Fig. 2 (A) Detailed bathymetric map showing bathymetry around YK13-08 Shinkai dives 1363 and 1364 and location of Shinkai Seep Field (SS) (Ohara *et al*. 2012). (B) IMI30 sidescan sonar image of region. High backscatter (outcrops) shown with darker shading, low backscatter (sediment cover) shown with lighter shading. '*' marks possible volcaniclastic ridge. (C) Photograph from Shinkai 6500 submersible showing typical seafloor observed during Dive 1363. Fragments and cobbles on seafloor are dominated by basaltic volcaniclastics like those studied here.

sonar imagery over the area (Martinez *et al*. 2012, Fig. 2B). Samples were collected during dive #1363 of the manned submersible Shinkai 6500 on September 10, 2013, as part of JAMSTEC research cruise of R/V Yokosuka (YK1308). The dive site was located about 11°38′N, 143°E, approximately 30 km north of the trench axis, some 7.5 km west of the Shinkai Seep Field (Ohara *et al*. 2012), and about 60 km ENE of the Challenger Deep (Fig. 2). This region is within the Mariana Trench Marine National Monument of the USA and our study was done under the special use permit #12541-12001. The dive traversed north up the inner wall of the Mariana Trench from 6094 to 5584 m below sealevel and was intended to search for additional forearc seeps and communities. An Eocene-aged arc-related gabbro was found in this area (Y. Ohara, unpublished data). This gabbro illustrates that this area has crustal blocks with Eocene to Miocene aged volcanics. Previous studies suggest that the Moho is exposed at approximately 5500 mbsl near the study area, so we expected to recover peridotites. A total of 18 samples were collected during this dive, consisting of peridotites and moderately lithified volcaniclastic sediments (hyaloclastities), composed of sand-sized, reddish-brown matrix with pieces of basaltic glass up to 2 cm across (Fig. 3). Three samples of volcaniclastic sediment (#12541-12001-YK13-08-6K-1363-R05, R06, and R15; hereafter for simplicity 1363-R05, R06, 15) from Shinkai dive 1363 were studied (see Fig. 2 for locations). Dive 1364 continued the traverse up the slope (5608–5197 m; Fig. 2A) and encountered similar volcanic-rich sediments but these were much less common than peridotites.

The samples that we studied are all basaltic volcaniclastics. Our chemical studies focus on glass fragments but we also examined the texture and composition of the volcaniclastic matrix (Fig. 4). The matrix shows no lamination or bedding, is poorly sorted and well indurated, and we interpret the samples as fragments from a volcaniclastic, bottom-hugging gravity flow. These probably moved from the eruption site as laminar mass flows (Fisher 1984) and must have been deposited downhill from their eruption vent. We have no constraints about how many different pyroclastic flows were sampled. Because the three samples we examined are similar in appearance and contain basaltic glass of very similar composition, they could be from the same flow. Also, we have no constraints on the width or thickness of the volcaniclastic flow(s).

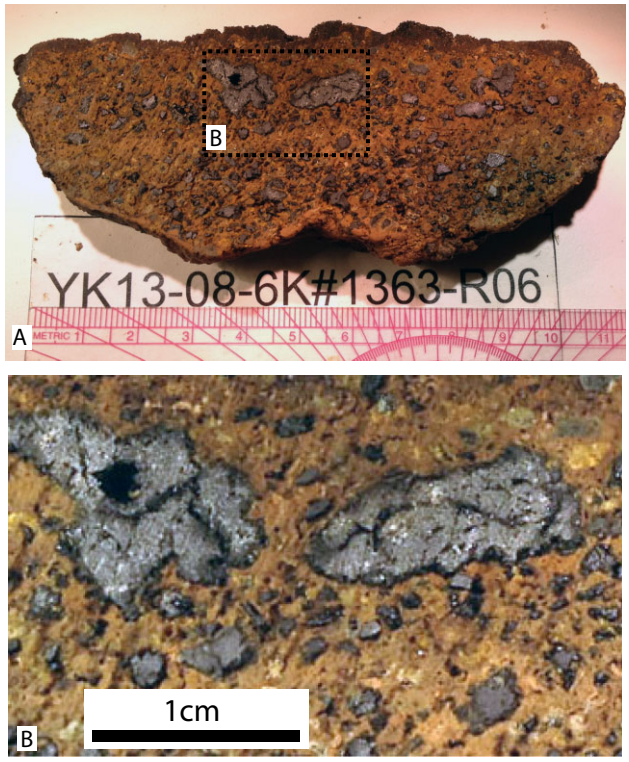

Fig. 3 Hand specimen of YK13-08 dive 1363 R06 volcaniclastic sediment, entire section (A) and close-up (B). Note that most of the visible fragments appear to be glassy basalts.

The volcaniclastic matrix is full of rock and mineral fragments of various shapes and sizes, including delicate fragments such as those highlighted with yellow 'D' in Figure 4. Such delicate fragments are unlikely to have suffered much buffeting from grain-to-grain contacts during transport, and must have been supported during transport downslope by the strength and buoyancy of the matrix. We infer that the volcaniclastic deposit formed as a submarine mudflow or lahar as it moved downslope from the eruption site. One sample (1364-R03) is a harzburgite with a 4 cm thick semi-lithified muddy volcanic sandstone rim, suggesting that the harzburgite may have been a clast dislodged in the vent or picked up during volaniclastic flow. Although palagonite is common in the matrix, the glass fragments are fresh and unaltered. Manganese coating on volcaniclastic samples is thin to nonexistent, and we infer from this and freshness of glass fragments that the flow occurred sometime in the last million years.

ANALYTICAL METHODS

Glass fragments, microlites in glass fragments, and matrix components were studied. Rock

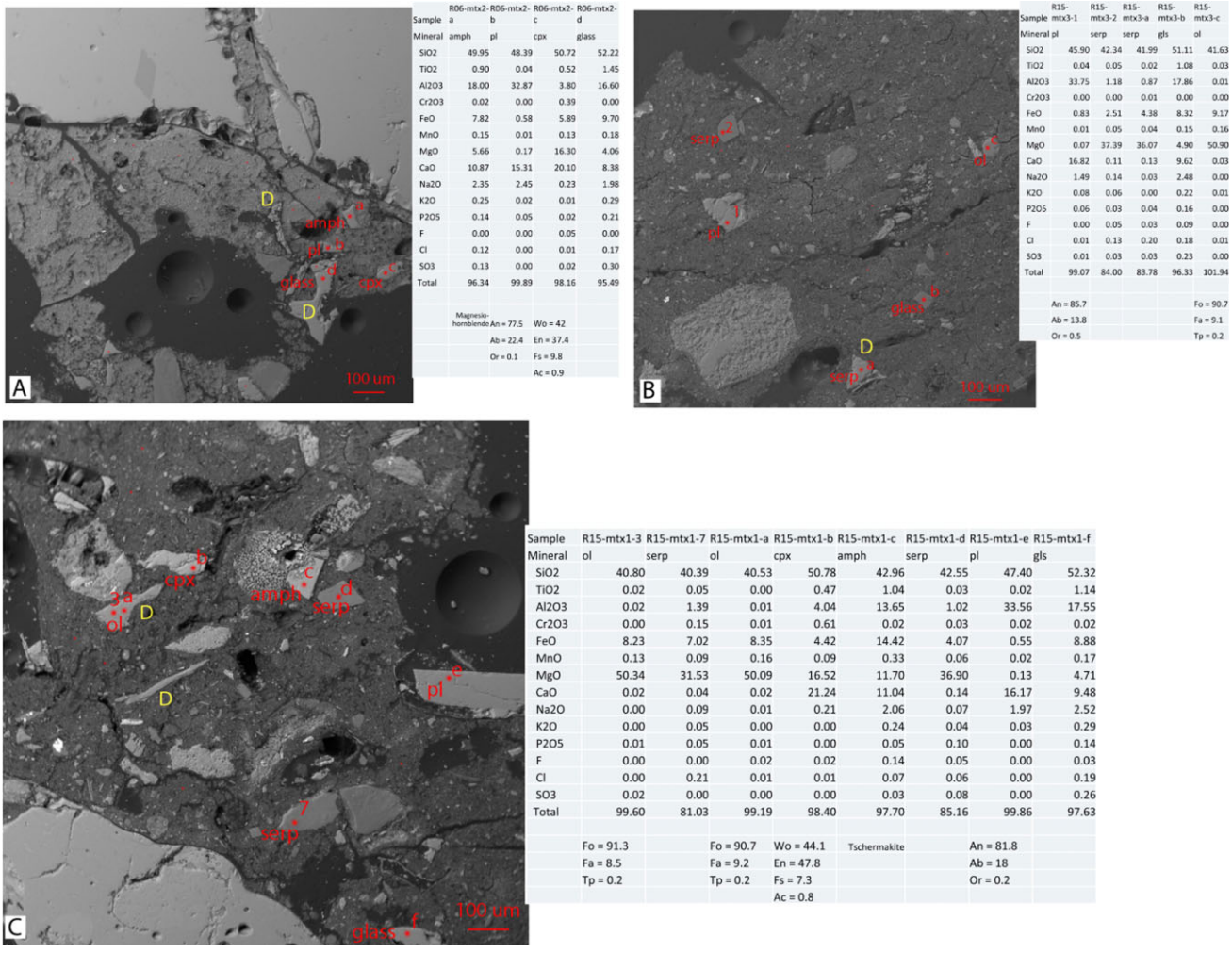

Sample	R06-mtx2-a	R06-mtx2-b	R06-mtx2-c	R06-mtx2-d
Mineral	amph	pl	cpx	glass
SiO2	49.95	48.39	50.72	52.22
TiO2	0.90	0.04	0.52	1.45
Al2O3	18.00	32.87	3.80	16.60
Cr2O3	0.02	0.00	0.39	0.00
FeO	7.82	0.58	5.89	9.70
MnO	0.15	0.01	0.13	0.18
MgO	5.66	0.17	16.30	4.06
CaO	10.87	15.31	20.10	8.38
Na2O	2.35	2.45	0.23	1.98
K2O	0.25	0.02	0.01	0.29
P2O5	0.14	0.05	0.02	0.21
F	0.00	0.00	0.05	0.00
Cl	0.12	0.00	0.01	0.17
SO3	0.13	0.00	0.02	0.30
Total	96.34	99.89	98.16	95.49
	Magnesio-hornblende	An = 77.5	Wo = 42	
		Ab = 22.4	En = 37.4	
		Or = 0.1	Fs = 9.8	
			Ac = 0.9	

Sample	R15-mtx3-1	R15-mtx3-2	R15-mtx3-a	R15-mtx3-b	R15-mtx3-c
Mineral	pl	serp	serp	gls	ol
SiO2	45.90	42.34	41.99	51.11	41.63
TiO2	0.04	0.05	0.02	1.08	0.03
Al2O3	33.75	1.18	0.87	17.86	0.01
Cr2O3	0.00	0.00	0.01	0.00	0.00
FeO	0.83	2.51	4.38	8.32	9.17
MnO	0.01	0.05	0.04	0.15	0.16
MgO	0.07	37.39	36.07	4.90	50.90
CaO	16.82	0.11	0.13	9.62	0.03
Na2O	1.49	0.14	0.03	2.48	0.00
K2O	0.08	0.06	0.00	0.22	0.01
P2O5	0.06	0.03	0.04	0.16	0.00
F	0.00	0.05	0.03	0.09	0.00
Cl	0.01	0.13	0.20	0.18	0.01
SO3	0.01	0.03	0.03	0.23	0.00
Total	99.07	84.00	83.78	96.33	101.94
	An = 85.7				Fo = 90.7
	Ab = 13.8				Fa = 9.1
	Or = 0.5				Tp = 0.2

Sample	R15-mtx1-3	R15-mtx1-7	R15-mtx1-a	R15-mtx1-b	R15-mtx1-c	R15-mtx1-d	R15-mtx1-e	R15-mtx1-f
Mineral	ol	serp	ol	cpx	amph	serp	pl	gls
SiO2	40.80	40.39	40.53	50.78	42.96	42.55	47.40	52.32
TiO2	0.02	0.05	0.00	0.47	1.04	0.03	0.02	1.14
Al2O3	0.02	1.39	0.01	4.04	13.65	1.02	33.56	17.55
Cr2O3	0.00	0.15	0.01	0.61	0.02	0.03	0.02	0.02
FeO	8.23	7.02	8.35	4.42	14.42	4.07	0.55	8.88
MnO	0.13	0.09	0.16	0.09	0.33	0.06	0.02	0.17
MgO	50.34	31.53	50.09	16.52	11.70	36.90	0.13	4.71
CaO	0.02	0.04	0.02	21.24	11.04	0.14	16.17	9.48
Na2O	0.00	0.09	0.01	0.21	2.06	0.07	1.97	2.52
K2O	0.00	0.05	0.00	0.00	0.24	0.04	0.03	0.29
P2O5	0.01	0.05	0.01	0.00	0.05	0.10	0.00	0.14
F	0.00	0.00	0.02	0.02	0.14	0.05	0.00	0.03
Cl	0.00	0.21	0.01	0.01	0.07	0.06	0.00	0.19
SO3	0.02	0.00	0.00	0.00	0.03	0.08	0.00	0.26
Total	99.60	81.03	99.19	98.40	97.70	85.16	99.86	97.63
	Fo = 91.3		Fo = 90.7	Wo = 44.1	Tschermakite		An = 81.8	
	Fa = 8.5		Fa = 9.2	En = 47.8			Ab = 18	
	Tp = 0.2		Tp = 0.2	Fs = 7.3			Or = 0.2	
				Ac = 0.8				

Fig. 4 Electron backscatter images of millimeter-sized expanses of volcaniclastic matrix, with chemical analyses by EMP of selected fragments (minerals and glass) listed to the right of each image. Delicate fragments suggesting massive debris flow is shown by yellow 'D'. (A) 1363-R06, with fragments of (a) hornblende, (b) bytownite, (c) clinopyroxene, and (d) glass. (B) 1363-R15, with fragments of (1) plagioclase, (2, a) serpentinite, (b) glass, and (c) olivine. (C) 1363-R15, with fragments of (3, a) olivine, (7, d) serpentinite, (b) clinopyroxene, (c) amphibole, (e) plagioclase, and (f) glass.

samples were examined using electron backscatter imaging and this allowed us to determine major element compositions of mineral phases and glass fragments using the electron microprobe at U Nevada Las Vegas using a JAX8900 electron microprobe analyzer equipped with four wavelength-dispersive spectrometers. Basaltic volcaniclastics and matrix were placed in 1′ epoxy mount and polished and carbon-coated prior to analyses. Elements Si, Ti, Al, Cr, Fe, Mn, Mg, Ca, Na, K, P, F, Cl and S were analyzed at 15 keV acceleration voltage, beam current 10 nA, defocused beam of 20 micrometers for glasses, with a peak counting time of 10 s for Na and 30 s for other elements. For mineral grains, beam condition was 15 keV acceleration voltage, 20 nA beam current, defocused beam of 10 micrometers, with a peak counting time of 20 s for Na and 30 s for other elements. Since the high-Si glass fragments are about 10 to 15 micrometers across, the beam size had to be set at 10 micrometers, possibly leading to loss of Na. Calibration standards used for glass analyses were: Smithsonian VG2 basaltic glass for Si and Ca, almandine for Al, chromite for Cr, ilmenite for Ti, pyrope for Fe and Mg, rhodonite for Mn, albite for Na, microcline for K, apatite for P, fluorite for F, AgCl for Cl, and barite for S. For high Si glass, Smithsonian tektite glass was used for Si calibration. For mineral grains in matrix, Si, Al, and Ca, used Smithsonian plagioclase for calibration.

Water and CO_2 contents in one chip from each of three samples were determined by Fourier Transform Infrared (FTIR) spectroscopy at the Graduate School of Oceanography, University of Rhode Island, using a Thermo Nicolet iS50 bench FTIR

coupled with a Continuum IR microscope. The sample area was purged with dry, CO_2-free air to minimize atmospheric interferences, and analytical conditions used a custom aperture that varied from 100×100 μm to 60×60 μm, depending on crystallinity of the matrix glass. Data were collected in transmission using a 250 μm MCT-A detector, and reduced following methodologies outlined by Kelley and Cottrell (2012). Owing to the microcrystalline nature of these glasses, thin wafer preparation (30–40 μm) was required for two glasses in order to expose enough optically clear glass for volatile analysis, rendering dissolved CO_3^{2-} below detection.

Trace element abundances were determined by Laser Ablation Inductively-Coupled Plasma Mass Spectrometry (LA-ICP-MS) at the Graduate School of Oceanography, University of Rhode Island, using a Thermo X-Series 2 quadrupole ICP-MS coupled with a New Wave UP213 Nd-YAG laser ablation system. Data were collected using 80 μm spots and a 5 Hz repeat rate, normalized to ^{43}Ca as the internal standard, and calibrated against eight natural-composition reference glasses from the USGS and MPI-DING series (BCR-2G, BIR-1G, BHVO-2G, KL2-g, ML3B-g, StHls-g, T1-g, GOR-132-g), following methods outlined by Kelley *et al.* (2003) and Lytle *et al.* (2012).

RESULTS

Complete microprobe analyses are provided in Document S1 (major element compositions of glass fragments), Document S2 (compositions of minerals in glass), and Document S3 (compositions of small minerals and rock fragments in matrix). These results are discussed in order of glass, minerals in glass, and minerals in matrix below.

A total 153 major element analyses of 14 fragments were carried out for 1363-R05, 131 analyses of 13 fragments for 1363-R06, and 145 analyses of 13 fragments from 1363-R15 were carried out, for a total of 429 analyses. These analyses gave very similar compositions, indicating that the glass fragments are basalt (Table 1). Analytical totals are consistently approximately 97.5–98%, suggesting the presence of considerable (about 2 wt.%) water and other magmatic volatiles, similar to what is reported for BAB tholeiites (Kelley *et al.* 2006). The composition of these glasses are otherwise remarkably MORB-like (Table 2), especially in terms of low abundances of incompatible major elements: TiO_2, Na_2O, and K_2O. These characteristics of Dive 1363 basaltic glasses are comparable to basaltic rocks from the SE segment of the SE Mariana Forearc Rift (SE-SEMFR) to the east, which erupted in a comparable near-trench position to that of the Dive 1363 basaltic glass samples (Fig. 1B, Table 1; Ribeiro *et al.* 2013a,b).

Abundances of magmatic H_2O and CO_2 in glass fragments are also presented in Table 1. Dive 1363 basalt glasses contain 1.97–2.29 wt.% H_2O and 94 ppm CO_2 for the one sample with detectable dissolved CO_2^-. Volatile (H_2O-CO_2) saturation pressure for this sample, as modeled using VolatileCalc (Newman & Lowenstern 2002) is 642 bars, the calculated saturation pressure is very deep compared to any spreading center. The saturation depth is consistent with a hydrostatic eruption depth of 6545 m, which is near the collection depth of the sample. The fact that the carbon dioxide is not completely outgassed suggests that magmatic water did not outgas significantly and that the mean of 2.1 wt.% H_2O is a useful approximation of the water content in the basaltic magma when it erupted. This is much higher H_2O contents than found in most MORB glasses and is the single most important way that MORB and Dive 1363 glasses differ; primitive NMORB contains approximately 0.15% H_2O (Michael 1995), less than 10% of what the 1363 basalts contain. Dive 1363 glasses are very similar to the one sample of SE-SEMFR basalt glass analyzed for water and CO_2 (J. Ribeiro, personal communication).

Dive 1363 glasses have Mg# (=100Mg/Mg + total Fe) ranging from 52 to 57, significantly lower than Mg# ca. 65, expected for unfractionated, primitive basalts. Dive 1363 glass fragment Mg# is similar to that of MORB and SE-SEMFR basalt, all of which show similar extents of fractionation. CIPW norms (Table 1) indicate that Dive 1363 basalts are quartz-normative tholeiites, similar to SE-SEMFR basalts but differing from typical MORB, which is often olivine-normative basalt.

Trace element concentrations for the three Dive 1363 basaltic glass samples are listed in Table 2, along with some key trace element ratios and mean compositions of SE-SEMFR basalt and MORB. Dive 1363 basalts have chondrite-normalized Rare Earth Element (REE) patterns with concave-downward patterns and modest light REE depletions (Fig. 5). These REE patterns are very similar to those of MORB and SE-SEMFR basalts. All three Dive 1363 glasses show maxima in the middle REE (Nd – Gd) – also like SEMFR and MORB; and all three show a modest decrease

Table 1 Major element analyses of YK1308 Dive 1363 basaltic glass fragments

	1363-R05		1363-R06		1363-R15		SE-SEMFR Mean Glass[†]		ALL MORB[§]	
	Mean	stdev	Mean	stdev	Mean	stdev	Mean	stdev		
N	153		131		145		6		430	
SiO_2	51.00	0.39	51.37	0.42	51.94	0.25	51.48	0.91	50.47	0.08
TiO_2	1.01	0.07	1.10	0.06	1.14	0.05	1.03	0.19	1.68	0.05
Al_2O_3	16.38	0.27	16.38	0.28	16.46	0.64	15.73	0.27	14.70	0.12
Cr_2O_3	0.01	0.01	0.01	0.01	0.01	0.01				
FeO[†]	8.23	0.31	8.66	0.25	8.85	0.34	8.53	0.70	10.43	0.21
MnO	0.15	0.02	0.16	0.02	0.16	0.02	0.15	0.02	0.18	0.01
MgO	6.17	0.52	5.59	0.64	5.36	1.28	5.62	0.86	7.58	0.12
CaO	11.01	0.56	10.34	0.68	10.08	0.27	10.05	1.08	11.39	0.09
Na_2O	2.88	0.19	3.07	0.22	3.20	0.10	3.22	0.46	2.79	0.03
K_2O	0.22	0.02	0.23	0.04	0.26	0.01	0.25	0.05	0.16	0.01
P_2O_5	0.11	0.02	0.12	0.03	0.12	0.03	0.11	0.03	0.18	0.01
F	0.03	0.04	0.02	0.04	0.03	0.05	0.02			
Cl	0.10	0.02	0.13	0.03	0.13	0.01	0.04			
SO_3	0.19	0.02	0.28	0.18	0.20	0.02	0.22			
Total	97.49		97.46		97.94		96.45		99.56	
H_2O (wt. %)	1.97	0.05	2.29		2.06	0.16	2.04[‡]		0.15[§]	
CO_2 (ppm)	455	116	539		94	22	51			
Mg#	57.2		53.5		51.9		54.0		56.4	
CIPW NORMS[¶]										
QZ	1.69		2.52		2.1		2.56			
PL	57		57.82		58.77		57.03		50.93	
OR	1.36		1.42		1.6		1.54		0.95	
DI	19.07		17.1		16.59		18.18		23.36	
HY	15.93		15.85		17.47		15.53		12.61	
OL									8.52	
IL	1.98		2.15		0.27		2.03		3.21	
MT	2.73		2.87		2.94		2.86			
AP	0.25		0.28		0.28		0.25		0.42	

[†] wt. %, calculated volatile free, Fe3+/total = 0.2; adjusted to total 100%. [‡] Ribeiro *et al*., 2013b; volatiles from Ribeiro *et al*. submitted. [§] Gale *et al*. 2013. [¶] Michael 1995.

in the heavy REE, from Tb to Lu. Extended trace element patterns (spider diagrams; Fig. 6) emphasize strong similarities and subtle differences between Dive 1363 glasses and SE-SEMFR basalts on the one hand and MORB on the other. One significant difference is that Dive 1363 basalts have a modest negative Nb–Ta anomaly (Th/Nb = approx. 0.1) whereas MORB generally does not (Th/Nb = 0.08). In addition, Dive 1363 samples have a somewhat higher ratio of fluid-mobile incompatible elements (e.g. Rb) relative to similarly incompatible but fluid-immobile elements (e.g. Zr) than do MORB (Table 2). There are also indications from lower Ti/V that Dive 1363 magmas originated from a somewhat more oxidized mantle source region than do most MORB (Table 2).

Small crystals of plagioclase and clinopyroxene occur in the glasses. Plagioclase in all three samples is mostly bytownite. 27 analyses of plagioclase in R05 yields a range of An67-83, mean = An74.7 ± 3.6 (1 standard deviation). 26 analyses of plagioclase in R06 yields a range of An68-95, mean = An77.8 ± 9. 46 analyses of plagioclase in R15 yields a range of An67-88, mean = 77.2 ± 7. Clinoyroxene in all three samples is anhedral augite with similar compositions. 18 analyses of one clinopyroxene in R05 yielded Wo43.4 ± 2.3 En46.5 ± 1.7 Fs9.2 ± 1.2 Ac0.9 ± 0.16. Eight analyses of one clinopyroxene in R06 yielded a mean of Wo43 ± 2 En47 ± 2 Fs9 ± 1 Ac0.8 ± 0.2. Twelve analyses of clinopyroxene in R15 yielded a mean of Wo42 ± 2 En47 ± 2 Fs10 ± 0.75 Ac0.9 ± 0.35. The compositions of plagioclase and clinopyroxenes in all three samples are essentially identical. These mineral compositions indicate crystallization from fractionated magma. There is one anhedral amphibole and one anhedral ilmenite found in one R15 basaltic glass fragment, the amphibole can be classified as Tschermakite.

Rock and mineral fragments in the volcaniclastic matrix include olivine, orthopyroxene, serpentine, epidote, amphibole, magnetite, clinopyroxene, plagioclase, quartz, basaltic glass, and

Table 2 Trace element contents of YK1308 Dive 1363 basaltic glass

	1363 – R05	1363 – R06	1363 – R15	mean SE-SEMFR†	All MORB‡
V (ppm)	278	275	261	236	309
Cr	26	28	21	22	249
Ni	30.7	29.6	27.4	19.7	92
Rb	3.55	3.67	3.46	3.72	2.88
Sr	167	169	170	179	129
Y	22.1	23.3	25.8	21.9	36.8
Zr	82.5	85.7	93.6	77.8	117
Nb	2.71	2.73	2.72	1.91	5.24
Cs	0.09	0.08	0.08	0.1	0.034
Ba	41.6	40.9	40.2	47	29.2
La	3.63	3.57	3.88	3.34	5.21
Ce	10.9	10.7	10.5	9.2	14.9
Pr	1.67	1.68	1.73	1.5	2.24
Nd	8.31	8.49	9.14	7.91	12
Sm	2.72	2.84	2.97	2.57	3.82
Eu	1.02	1.06	1.08	0.94	1.36
Gd	3.45	3.56	3.97	3.55	4.99
Tb	0.58	0.64	0.69	0.61	0.90
Dy	3.79	4.03	4.4	3.88	6.08
Ho	0.82	0.89	0.97	0.83	1.28
Er	2.29	2.52	2.76	2.34	3.79
Tm	0.35	0.39	0.42	0.35	
Yb	2.33	2.41	2.58	2.29	3.63
Lu	0.34	0.35	0.41	0.33	0.53
Hf	1.75	2.03	2.12	1.89	2.79
Ta	0.16	0.17	0.18	0.12	0.34
Pb	0.89	0.85	0.73	0.83	0.57
Th	0.28	0.27	0.3	0.24	0.40
U	0.14	0.14	0.12	0.10	0.12
K/Rb	607	565	600	558	461
Rb/Zr	0.04	0.04	0.04	0.05	0.02
Ti/V	24.3	24.4	25.2	19.1	32.6
La/Nb	1.34	1.31	1.43	1.75	0.99
Nb/Yb	1.16	1.13	1.05	0.83	1.44
Pb/Ce	0.082	0.079	0.070	0.090	0.038
Th/U	2.00	1.93	2.50	2.40	3.33
La/Nd	0.44	0.42	0.42	0.42	0.43
Th/La	0.08	0.08	0.08	0.07	0.08
Th/Nb	0.10	0.10	0.11	0.13	0.08

† Ribeiro *et al.* 2013a,b. ‡ Gale *et al.* 2013.

high-Si glass. Electron microprobe analyses are listed in Document S3.

A total of 71 fragments in R05 matrix were analyzed. We idenitified four olivines (Fo 90.6–91.6), one orthopyroxene (Wo5.3 En71.4 Fs23.2 Ac0.2), one epidote, one amphibole (Magnesio-hornblende), four magnetite, one high-Si glass, 26 clinopyroxenes, 23 plagioclases, and eight basaltic glasses. Excepting four sodic plagioclases (An6-49), all other plagioclases (An 67–91), clinopyroxenes (En38-45), and basaltic glasses are similar to those in the large basaltic glass and the included plagioclase and clinopyroxene.

Twenty six fragments were analyzed in the R06 matrix. There are two olivines (Fo78 and Fo81),

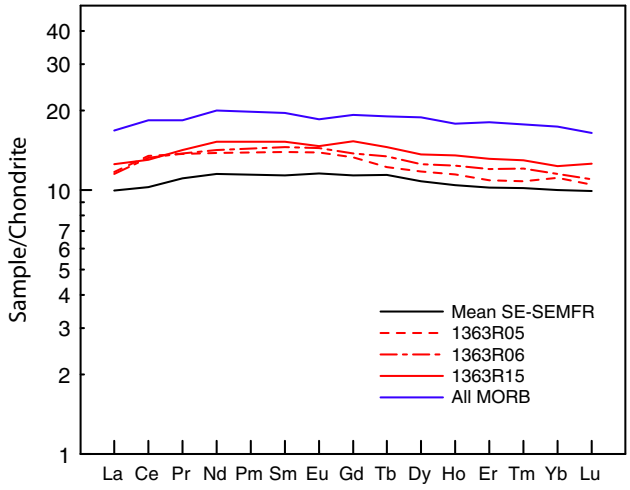

Fig. 5 Chondrite-normalized REEs pattern for three Dive 1363 glasses listed in Table 3. Mean compositions of 'All MORB' (Gale *et al.* 2013) and mean SEMFR basalt (Ribeiro *et al.* 2013b) are also plotted for comparison. Concentrations are normalized to chondrite abundances of Boynton (1985).

one serpentine, one quartz, seven clinopyroxene (En 38–47), six plagioclase (An73-86), nine basaltic glasses. The olivine is different from olivines from R05 and R15 samples. All plagioclases, clinopyroxenes, and basaltic glasses are similar to the large basaltic glass and the included plagioclase and clinopyroxene.

Forty five fragments were analyzed in R15 matrix. There are seven olivine (Fo90-92), six serpentine, one epidote, two amphibole, eight clinopyroxene (En41-45), eight plagioclase, 10 basaltic glass, and one high-Si glass. R15 olivine (Fo >90) is identical to R05 olivine, but different from R06 olivine (Fo78-81). R15 matrix clinopyroxene (En41-45) is slightly different from clinopyroxene in basaltic glass, the matrix clinopyroxene have higher Al_2O_3 and TiO_2 than clinopyroxene in basaltic glass. There are two high Na plagioclase grains (An43-56), other plagioclases (An73-85) are similar to the plagioclase in basaltic glass. There are two basaltic glass grains that have higher MgO (15.4–16.6 wt%) and lower Al_2O_3 (4.9-6.2 wt%) than other basaltic glasses, which are similar to the large basaltic glasses (Al_2O_3 ~16–17 wt%, MgO ~4–6 wt%).

DISCUSSION

The MORB-like composition of the YK13-08 Shinkai Dive 1363 glasses that we have analyzed indicate derivation from melting of oceanic asthe-

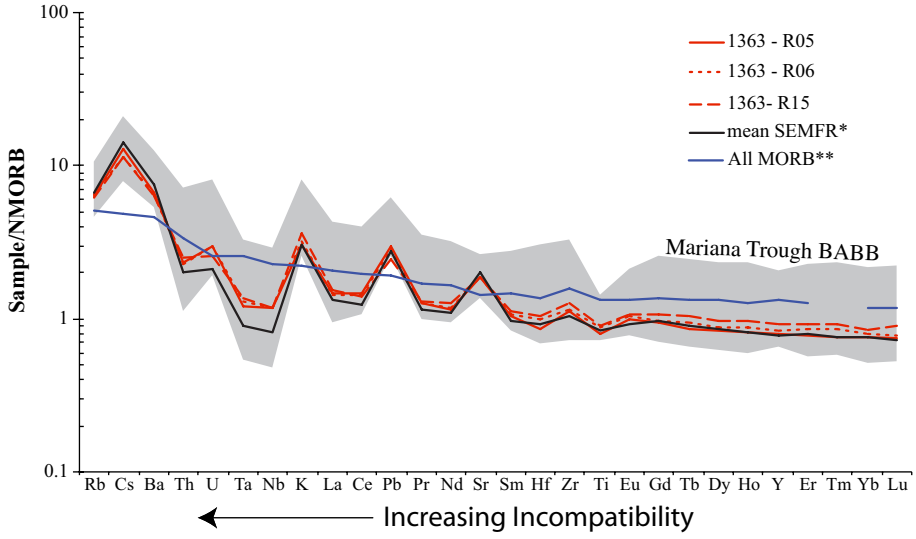

Fig. 6 Extended trace element diagram for 1363 glasses compared with patterns for 'Mean SE-SEMFR' (Ribeiro *et al.* 2013a) and 'All-MORB' (Gale *et al.* 2013). Grey field is Mariana Trough BABB from Brounce *et al.* (in press). Normalizing abundances and element order from Sun and McDonough (1989).

nosphere, but it is surprising that such melts were generated so close to the deepest trench on Earth.

These results are intriguing but more work is needed to determine the extent of young BAB igneous activity near the Challenger Deep before we can understand its significance. Here we briefly discuss three implications of our results: (i) What was the eruptive style and where did the eruption occur? (ii) What are the petrogenetic implications of Dive 1363 basalts? and (iii) What are the implications of our results for future studies of the region?

ERUPTION STYLE AND VENT LOCATION

The three rock samples that we studied formed by a frothy eruption of basaltic magma that was broadly MORB-like but with high water and which may have contained high SO_2 and/or CO_2 contents prior to eruption. We calculated temperatures for plagioclase-glass and cpx-glass using the Putirka (2008) thermometer spreadsheet, using average glass compositions for each sample. There is a good agreement between pl-glass (R05 approx. 1130°C; R06 approx. 1110°C; R15 approx. 1120°C) and cpx-glass (R05 approx. 1180°C; R06 approx. 1170°C; R15 approx. 1160°C) pairs for all three samples (Document S4) and this range (1110°–1180°C) is taken to approximate the magma temperature at the time of eruption. This magma degassed vigorously as it erupted. We have no direct information about where the eruption occurred, but because these are laminar density flows (lahars), they must have originated somewhere upslope along the inner trench wall to the north of where they were collected. They could not have originated from the north side of the S. Mariana Forearc Ridge (Fig. 1B), and it is difficult to imagine how such a volcaniclastic flow could have originated from north of the ridge that lies a few km north of the detailed study area. For this reason, we think that the eruption site must lie on this bathymetric high ('*' in Figs 1B,7). Regional HMR-1 sonar backscatter imagery (Fryer *et al.* 2003) over the region (Fig. 7A) shows no obvious volcanic features around the dive site, but the entire trenchward slope is characterized by high backscatter, indicating steep slopes of lightly sedimented basement. There is a low backscatter region surrounding the local forearc high labeled with an '*' in Figure 7. Deep towed IMI-30 sidescan sonar imagery of the dive area (Fig. 2) also does not give clear indications of young local volcanic structures, but a lobate ridge (marked with '*' in Fig. 2) could be a volcaniclastic flow. Basement morphology indicates generally low sediment thickness with local ponds (lighter grey areas, Figs 2B,7A). Imaged lobe-like morphologies may be landslide or debris flow fronts.

HMR-1 shallow towed sidescan sonar imagery show generally high backscatter in the area (Fig. 7A) with local patches of low backscatter. This suggests that that the area is floored by lightly sedimented basement with small local sediment ponds. Compiled bathymetry (Fig. 7B), however shows several ridges above the 4000 m

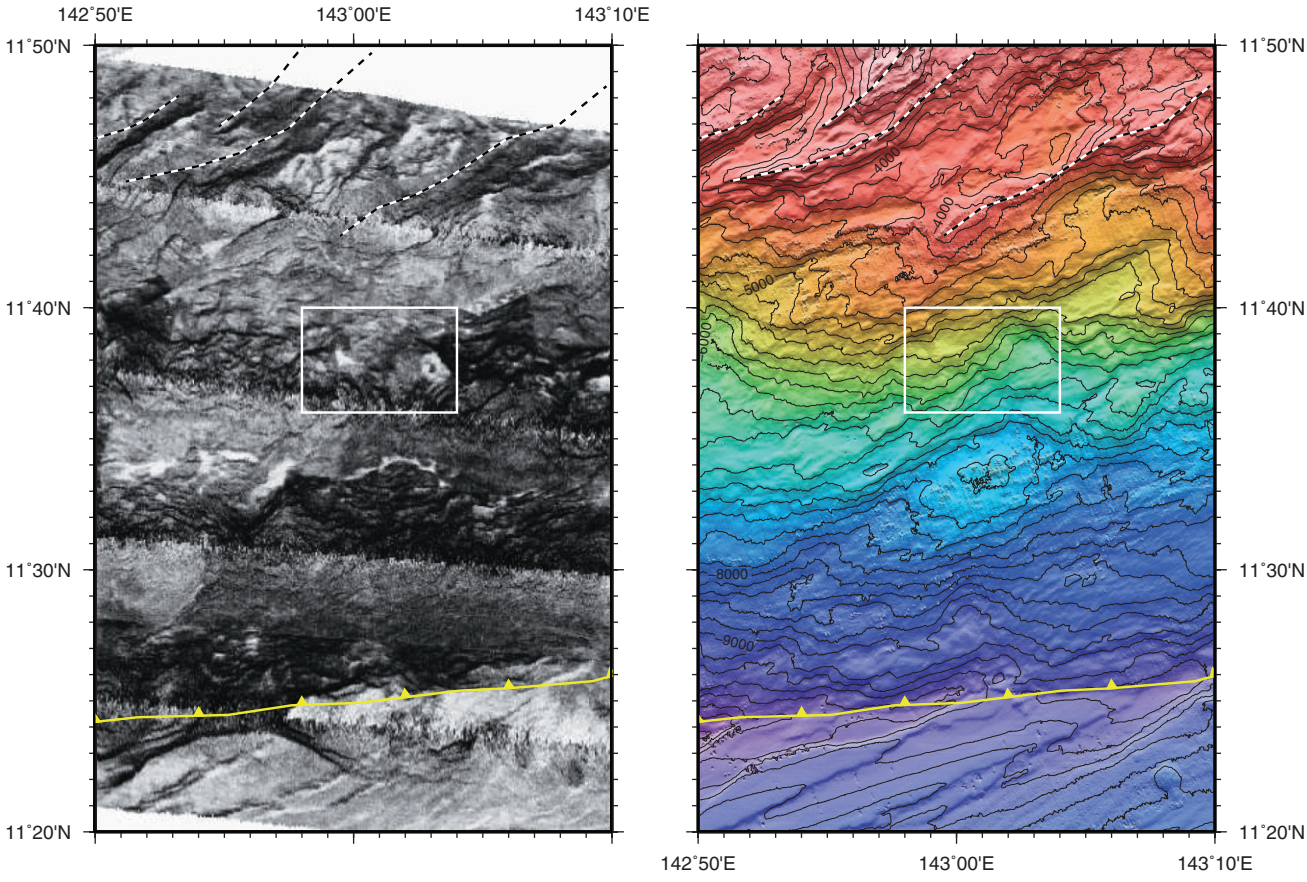

Fig. 7 (A) HMR-1 sonar backscatter imagery from R/V Melville cruise MV0101 over part of southern Mariana margin (location shown in Fig. 1B). (B) Detail of bathymetry; compilation described in Figure 1 shown with 200 m contours. White box shows location of Figure 2; Trench axis indicated with yellow barbed line. Possible volcanic ridges that may be sources of volcaniclastics indicated with dashed lines. In A, dark areas correspond to high backscatter, generally indicating a high insonification angle and/or bare or lightly sedimented basement. Light areas indicate low backscatter and are generally due to low insonification angles, acoustic shadows and/or sediment-covered basement. Volcaniclastics generally accumulate in local flats and deeps. Sidescan nadir tracks trend approximately E-W and have a poorly imaged speckle character. See Fryer *et al.* (2003) for further details on sidescan acquisition and processing.

depth contour trending NE–SW. The relatively symmetric flank slopes of the ridges, their slightly higher backscatter compared to surrounding basement and locally broader and rounded mounds in places suggest that these are volcanic ridges, perhaps emplaced along fissure systems. These volcanic ridges may thus be the eruptive sources of the hyaloclastites as they are located proximal to and directly upslope of the sample sites.

We note that the volatile saturation pressure of the glass from 1363-R15, which has reliable H_2O contents, suggests a much higher eruption pressure, closer to 6 km. This suggests that the magma erupted so rapidly that it did not have time to fully degas before quenching, or the vent is closer to the dive site than we propose above. The preservation of delicate fragments also suggests a nearby eruption site. Clearly more work is needed to identify the eruption site.

The eruption was sufficiently violent to be something like a version of a deepwater (>3km) 'Strombolian-style' eruption. At pressures lower than that for mixed SO_2–CO_2–H_2O fluid saturation, magmas that are rich in these volatiles are likely to erupt more explosively than will fluid-poor magmas such as normal MORB. Violent deepwater eruptions are poorly known, but such an eruption style is required for fragmenting and quenching the erupting basaltic magma to form glass. Because the ridge to the north is as shallow as 3 km and samples were collected from as deep as 6 km, the eruption must have occurred at 300–600 bars hydrostatic pressure. Even at such pressures, mixed SO_2–CO_2–H_2O fluid can be oversaturated in basaltic magmas and SO_2 and CO_2 can begin to exsolve below the seafloor. The eruption that formed these volcaniclastic flows could have been like that recently observed at West Mata

volcano in the Lau Basin (Resing *et al.* 2011), although hydrostatic pressures resisting vesiculation and fragmentation would be significantly greater at the >3 km water depth of Mariana forearc eruption than at the ~1100 m eruption depth of W Mata (300 vs. 110 bars hydrostatic pressure).

Clearly the matrix was derived from several sources, principally basaltic magma but also incorporating fragments of the peridotite and older volcanic substrate. One source was the eruption itself, which provided fragments of basaltic glass and associated plagioclase and clinopyroxene (Fig. 4A–C). Contributions from ultramafic sources are also revealed by fragments of Fo90 olivine and serpentinite (Fig. 4B,C). High silica glass and amphibole grains (Fig. 4A,C) probably sample underlying Miocene volcanics. We also identified fragments of high Si glasses, SiO_2 71–73%, along with albite, several grains of andesine, and some epidote. No evidence of organisms was found in the matrix.

It seems likely that the fragments of peridotite xenocrysts and serpentinite fragments found in the volcaniclastic matrix could have been torn off the vent walls accompanying sub-seafloor exsolution of magmatic volatiles. The presence of Fo 91 olivine and serpentine in the matrix suggests that these flows might be akin to peperite, which form when magma and sediment explosively interact to produce volcaniclastic deposits. However, in this case, at least some of the matrix may reflect magma-serpentinized peridotite or magma-serpentine mud interaction. It is also possible that non-basaltic fragments were picked up from rock exposures during lahar flow. Fragmentation was rapid enough and transport distance was short enough that sufficient heat was retained by fragments to partially lithify (anneal) the deposit after it came to rest.

PETROGENETIC IMPLICATIONS

As noted above, Dive1363 glasses are broadly MORB-like – although they are more aluminous and marginally lower in TiO_2 compared to MORB – but with unusually high abundances of magmatic water. Some trace element ratios are MORB-like, for example La/Nd = 0.42–0.44. The similarity is also clear from chondrite-normalized REE patterns (Fig. 5). Major and trace element compositions of the three Dive 1363 samples are remarkably similar to each other and to basalts from SEMFR to the east and to global MORB (All-MORB of Gale *et al.* 2013).

Dive 1363 basalts show extended trace element patterns (spider diagrams; Fig. 6) that are similar to those of SE-SEMFR basalts to the east. This serves to further emphasize the strong similarities and subtle differences between Dive 1363 glasses and SEMFR basalts on the one hand and MORB on the other. Major element compositions and REE patterns are remarkably similar for Dive 1363, SEMFR, and MOR basalts. One subtle difference with MORB is that Dive 1363 basalts show modest negative Nb–Ta anomalies (Th/Nb = ~0.1) whereas MORB generally does not (Th/Nb = 0.08). In addition, Dive 1363 basalts have a somewhat higher ratio of fluid-mobile incompatible elements like Rb and U relative to similarly incompatible but fluid-immobile Zr than do MORB (Table 2). There are also indications – based on lower Ti/V – that Dive 1363 magmas originated from a somewhat more oxidized mantle source region than do most MORB (Table 2; note that Ti/V also can vary with degree of melting and mantle depletion). Ti/V is thought to proxy for mantle oxidation state, with oxidized arc magmas having low Ti/V (<20) compared to higher values for more reduced MORB and OIB (20–100; Shervais 1982). Mean SE-SEMFR basalt has Ti/V = 19 but the three Dive 1363 basalt glasses have higher and more MORB-like Ti/V of 24–25.

La/Nb = 1.4 was argued by Condie (2001) to distinguish convergent margin lavas (with higher ratios) from basalts formed in other tectonic environments such as MORB and oceanic hotspots. The three samples of Dive 1363 basalt glass have La/Nb = 1.31–1.43, intermediate between All-MORB (La/Nb ~1) and mean SEMFR basalt (La/Nb = 1.75). Nb/Yb is thought to be a proxy for depletion of the mantle source, <~1 for depleted mantle, >~1 for undepleted or enriched mantle (Pearce 2008). Dive 1363 basalts have Nb/Yb = 1.05–1.16, somewhat lower than MORB (Nb/Yb = 1.44) but somewhat higher than mean SEMFR lavas (Nb/Yb = 0.83).

Pb/Ce is thought to track contributions from subducted sediments to the mantle source, with values approaching 0.5 for arc lavas (Miller *et al.* 1994), much higher than the Pb/Ce of MORB (approx. 0.04). The three samples of Dive 1363 glass have Pb/Ce approx. 0.08, much closer to MORB than to arc magmas and indicating a barely detectable contribution from subducted sediments. Plank (2005) argued that Th/La tracked sediment contributions, with mantle Th/La <0.20

and arc and sediments Th/La >0.20. The three samples of 1363 basalt, mean SEMFR, and global MORB have indistinguishable Th/La = 0.08, again indicating that subducted sediments contributed negligibly to the source of the 1363 basalt glasses. From all these considerations, we conclude that Dive 1363 basaltic glasses are largely indistinguishable from BAB basalts.

IMPLICATIONS FOR FUTURE RESEARCH

Volcaniclastics discovered by the Shinkai Dive 1363 (YK13-08 cruise) represent the second place in the southernmost Mariana forearc where we have found evidence of young basaltic volcanism close to the trench, the other being SEMFR, 130 km to the east. Igneous activity so close to a convergent plate margin is common only where BAB spreading ridges intersect the trench at Subduction–Transform Edge Propagators, or STEP faults (Govers & Wortel 2005). However, in these settings the lower plate motion at the trench is primarily transcurrent rather than convergent and these sites mark the lateral termination of subduction zones (Govers & Wortel 2005). The Challenger Deep forearc segment is not in a STEP fault geometry. What it has in common with STEP fault margins is active extension of the upper plate that advects asthenospheric mantle leading to melting and volcanism at the trench. Another difference from STEP fault margins is that upper plate extension at these margins is focused to narrow spreading centers whereas in the southern Mariana margin it is diffuse.

Identification of sites in the inner trench wall that erupt tholeiitic basalt demonstrate that BAB asthenosphere penetrates unusually far into the forearc and that lithosphere beneath the SMTTC is thin. Gvirtzman and Stern (2004) concluded that weak coupling between the downgoing Pacific plate and the overriding Mariana plate (facilitated by a slab tear beneath the West Santa Rosa Bank Fault, Fig. 1B) allowed the subducting plate to bend and sink more steeply than normally observed, and was an important contributing cause to the great depth of the trench here. The combined effects of rapid rollback, weak forearc lithosphere, and a narrow plate coupling zone makes it easy to stretch the upper plate so that a backarc basin extensional regime could extend into the trench region, albeit near-trench extension is characterized by diffuse magmatism and a plastic deformation style that is not well understood. Evaluating and refining these ideas and how SMTTC formation and deformation relates to the great depth of the Challenger Deep and the seafloor life that exists there should be an important geoscientific research focus for the 21st century. The technological challenges confronting such efforts will require international and interdisciplinary field, laboratory, and theoretical studies of what is happening on both sides of the Challenger Deep. On the Mariana margin, we need to look for more sites of recent volcanism in the inner trench wall. There are likely to be other sites of basaltic volcanism here that are yet to be discovered, and other regions of this forearc should be investigated for signs of volcanic activity. This includes summit regions of individual highs on the Southern Mariana Forearc Ridge as well as the N–S depression at 143°15′E (Fig. 1B). In addition, an OBS field program in the SMTTC is needed to define regions of shallow seismic activity, depth to the base of the lithosphere, and the geometry of the downgoing slab. Modeling studies to understand why the Challenger Deep forearc segment is so weak are needed to support these efforts. The Pacific plate south of the trench also needs to be swathmapped and geophysically investigated to see if evidence of unusually strong bending exists, such as outer trench normal faults and seismicity.

Finally, the proximity of the inferred volcanic source to the Shinkai Seep area opens the possibility that hydrothermal circulation was partly due to magmatic heat. We speculate that other sites of recent volcanism and serpentinite-hosted cold seeps exist in the region.

CONCLUSIONS

We have found a second site of young basaltic volcanism in the Challenger Deep forearc segment. Shinkai 6500 diving during YK13-08 (Dive 1363) recovered volcaniclastics from approx. 5.5 to 6 km deep in the inner wall of the Mariana Trench, approx. 50 km NE of the Challenger Deep. Abundant fragments of glassy fragments of tholeiitic basalts analyzed from three different samples are compositionally similar to MORB except for much higher contents of magmatic water (about 2% H_2O vs. < 0.2% H_2O in MORB) and spikes in trace element diagrams at Rb–Cs–Ba, K, Pb, and Sr. Dive 1363 basalt glasses are similar to basalts from SEMFR erupted near the trench and to basalts of the Mariana Trough backarc basin, and these melts may be derived from similar hydrous asthenosphere that underlies the southern Mariana

backarc basin and forearc. Basalt fragments and palagonitized matrix dominate the three samples we studied, but small xenocrysts and xenoliths derived from mantle peridotite and Neogene volcanics are also present, probably torn from the vent walls. Dive 1363 hyaloclastites erupted at 3–6 km water depth accompanied by vigorous degassing of volatiles, most likely CO_2. These results provide further evidence that the forearc adjacent to the Challenger Deep has been invaded by asthenospheric mantle and is composed of thin and weak lithosphere. Thin lithosphere of this region may result in weak coupling between the subducting Pacific Plate and overriding Mariana plate, which may be partly responsible for the great depth of the Challenger Deep.

ACKNOWLEDGEMENTS

Funding for this research includes NSF grant OCE-0961811 to Martinez; NSF OCE- 0961559 and NSF EAR- 1258940 to Kelley, and NSF-OCE 0961352 to Stern. This study was conducted under the special use permit #12541-12001 of US Fish and Wildlife Service for activities in the Mariana Trench Marine National Monument. We thank US Fish and Wildlife Service for approval of our study in the monument. We gratefully acknowledge the support of the crews of R/V Yokosuka and DSV Shinkai, R/V Thomas G. Thompson and the Hawaii Mapping Research Group without whom this research would have been impossible. We greatly appreciate the detailed comments of two anonymous referees and Associate Editor Ryuichi Shinjo.

REFERENCES

ARMSTRONG A. A. 2011. Cruise report USNS sumner, U.S. extended continental shelf cruise to map sections of the Mariana trench and the Eastern and Southern insular margins of Guam and the Northern Mariana Islands. [Cited 1 December 2013.] Available from: http://ccom.unh.edu/publications/Armstrong_2011_cruise_report_SU10-02_Marianas.pdf

BECKER N. C., FRYER P. & MOORE G. F. 2010. Malaguana-Gadao Ridge: Identification and implications of a magma chamber reflector in the southern Mariana Trough. *Geochemistry Geophysics Geosystems* **11**, Q04X13.

BIRD P. 2003. An updated digital model of plate boundaries. *Geochemistry Geophysics Geosystems* **4** (3), 1027. doi:10.1029/2001GC000252.

BOYNTON W. V. 1985. Chapter 3. Cosmochemistry of the rare earth elements: Meteorite studies. *In* Henderson P. (ed.) *Rare Earth Element Geochemistry Developments in Geochemistry*, Vol. 2, pp. 115–1522, Elsevier, Amsterdam.

BROUNCE M., KELLEY K. A. & COTTRELL E. in press. Variations in $Fe^{3+}/\Sigma Fe$ ratios of Mariana Arc basalts and primary fO_2 of the mantle wedge. *Journal of Petrology* (in press). doi:10.1093/petrology/egu065

CONDIE K. C. 2001. *Mantle Plumes and Their Record in Earth History*. Cambridge U. Press, Cambridge.

DVORKIN J., NUR A., MAVKO G. & BEN AVRAHAM Z. 1993. Narrow subducting slabs and the origin of backarc basins. *Tectonphysics* **227**, 63–79.

FISHER R. V. 1984. Submarine volcaniclastic rocks. *In* Kokelaar B. P. and Howells M. F. (eds.) *Marginal Basin Geology: Volcanic and Associated Sedimentary and Tectonic Processes in Modern and Ancient Marginal Basins*. Geological Society of London, Special Publication 16, pp. 5–27.

FRYER P. 1995. Geology of the Mariana Trough. *In* Taylor B. (ed.) *Backarc Basins: Tectonics and Magmatism*, pp. 237–79, Plenum Press, New York.

FRYER P., BECKER N., APPLEGATE B., MARTINEZ F., EDWARDS M. & FRYER G. 2003. Why is the Challenger Deep so deep? *Earth and Planetary Science Letters* **211**, 259–69.

GALE A., DALTON C. A., LANGMUIR C. H., SU Y. & SCHILLING J.-G. 2013. The mean composition of ocean ridge basalts. *Geochemistry Geophysics Geosystems* **14**, 489–518. doi:10.1029/2012GC004334.

GOVERS R. & WORTEL M. J. R. 2005. Lithosphere tearing at STEP faults: Response to edges of subduction zones. *Earth and Planetary Science Letters* **236**, 505–23.

GVIRTZMAN Z. & STERN R. J. 2004. Bathymetry of Mariana Trench-Arc system and formation of the challenger deep as a consequence of weak plate coupling. *Tectonics* **23**, TC2011. doi:10.1029/2003TC001581.

KATO T., BEAVAN J., MATSUSHIMA T., KOTAKE Y., CAMACHO J. T. & NAKAO S. 2003. Geodetic evidence of back-arc spreading in the Mariana Trough. *Geophysical Research Letters* **30**. doi:10.1029/2002GL016757.

KELLEY K. A. & COTTRELL E. 2012. The influence of magmatic differentiation on the oxidation state of Fe in a basaltic arc magma. *Earth and Planetary Science Letters* **329–-330**, 109–21.

KELLEY K. A., PLANK T., GROVE T. L., STOLPER E. M., NEWMAN S. & HAURI E. 2006. Mantle melting as a function of water content beneath back-arc basins. *Journal of Geophysical Research* **111**. doi:10.1029/2005JB003732.

KELLEY K. A., PLANK T., LUDDEN J. & STAUDIGEL H. 2003. Composition of altered oceanic crust at ODP 801 and 1149. *Geochemistry Geophysics Geosystems* **4**. doi:10.1029/2002GC000435.

KITADA K., SEAMA N., YAMAZAKI T., NOGI Y. & SUYEHIRO K. 2006. Distinct regional differences in crustal thickness along the axis of the Mariana Trough, inferred from gravity anomalies. *Geochemistry Geophysics Geosystems* **7**, Q04011.

LYTLE M. L., KELLEY K. A., HAURI E. H., GILL J. B., PAPIA D. & ARCULUS R. J. 2012. Tracing mantle sources and Samoan influence in the northwestern Lau back-arc basin. *Geochemistry Geophysics Geosystems* **13**, Q10019.

MARTINEZ F., FRYER P. & BECKER N. 2000. Geophysical characteristics of the southern Mariana Trough, 11°50′ N-13°40′ N. *Journal of Geophysical Research* **105**, 16591–607.

MARTINEZ F., KELLEY K. A. & STERN R. J. 2012. Creation and Deformation of Hydrous Lithosphere at the Southern Mariana Margin, Abstract EGU2012-6643, EGU General Assembly 2012, Wien.

MARTINEZ F. & TAYLOR B. 2003. Controls on backarc crustal accretion: Insights from the Lau, Manus and Mariana basins. *In* Larter R. and Leat P. (eds.) *Intra-Oceanic Subduction Systems: Tectonic and Magmatic Processes*. Geological Society of London, Special Publication 219, pp. 19–54.

MATSUDA T. & UYEDA S. 1971. On the Pacific type orogeny and its model – extension of the paired belts concept and possible origin of marginal seas. *Tectonophysics* **11**, 5–27.

MICHAEL P. 1995. Regionally distinctive sources of depleted MORB: Evidence from trace elements and H_2O. *Earth and Planetary Science Letters* **131**, 301–20.

MILLER D. M., GOLDSTEIN S. L. & LANGMUIR C. H. 1994. Cerium/lead and lead isotope ratios in arc magmas and the enrichment of lead in the continents. *Nature* **368**, 514–20.

NEWMAN S. & LOWENSTERN J. B. 2002. VolatileCalc: A silicate melt–H_2O–CO_2 solution model written in Visual Basic for Excel. *Computers & Geosciences* **28**, 597–604.

OHARA Y., REAGAN M. K., FUJIKURA K. *et al.* 2012. A serpentinite-hosted ecosystem in the Southern Mariana Forearc. *Proceedings of the National Academy of Science* **109**, 2831–5. http://www.pnas.org/cgi/doi/10.1073/pnas.1112005109.

PEARCE J. A. 2008. Geochemical fingerprinting of oceanic basalts with applications to ophiolite classification and the search for Archean oceanic crust. *Lithos* **100**, 14–48.

PLANK T. 2005. Constraints from thorium/lanthanum on sediment recycling at subduction zones and the evolution of the continents. *Journal of Petrology* **46**, 921–44.

PUTIRKA K. 2008. Thermometers and barometers for volcanic systems. *In* Putirka K. and Tepley F. (eds.) *Minerals, Inclusions and Volcanic Processes*, Reviews in Mineralogy and Geochemistry, Mineralogical Society of America 69, pp. 61–120.

RESING J. A., RUBIN K. H., EMBLEY R. W. *et al.* 2011. Active submarine eruption of boninite in the northeastern Lau Basin. *Nature Geoscience* **4**, 799–806.

RIBEIRO J., STERN R. J., KELLEY K. *et al.* 2013a. Nature and distribution of slab-derived fluids and mantle sources beneath the SE Mariana Forearc Rift. *Geochemistry Geophysics Geosystems* **14**, 4585–607. doi:10.1002/ggge.20244.

RIBEIRO J. M., STERN R. J., MARTINEZ F. *et al.* 2013b. Geodynamic evolution of a forearc rift in the southernmost Mariana Arc. *The Island Arc* **22**, 453–76.

SANDWELL D. T. & SMITH W. H. F. 1997. Marine gravity anomaly from Geosat and ERS 1 satellite altimetry. *Journal of Geophysical Research* **192**, 10039–54.

SHERVAIS J. W. 1982. Ti-V plots and the petrogenesis of modern and ophiolitic lavas. *Earth and Planetary Science Letters* **59**, 101–18.

STERN R. J., TAMURA Y., MASUDA H. *et al.* 2013. How does the Mariana Arc end in the south? *The Island Arc* **22**, 133–48.

SUN S. & MCDONOUGH W. F. 1989. Chemical and isotopic systematics of oceanic basalts: Implications for mantle composition and processes. *In* Saunders A. D. and Norry M. J. (eds.) *Magmatism in the Ocean Basins*. Geological Society of London, Special Publication 42, pp. 313–45.

SUPPORTING INFORMATION

Additional Supporting Information may be found in the online version of this article at the publisher's web-site:

Document S1 Electron microprobe glass analyses*.

Document S2 Electron microprobe analyses for minerals in glass clinopyroxene.

Document S3 Electron microprobe analyses for matrix minerals and rock fragments.

Document S4 Glass-Plagioclase and Glass-Clinopyroxene equilibration Temperatures.